Nuclear Inst. and Methods in Physics Research B 415 (2018) 9–16

Contents lists available at ScienceDirect

Nuclear Inst. and Methods in Physics Research B

journal homepage: www.elsevier.com/locate/nimb

GaAs low-energy X-ray radioluminescence nuclear battery

Zheng-Rong Zhang[a,1], Yun-Peng Liu[a,b,1], Xiao-Bin Tang[a,b,*], Zhi-Heng Xu[a], Zi-Cheng Yuan[a], Kai Liu[a], Wang Chen[a]

[a] Department of Nuclear Science and Engineering, Nanjing University of Aeronautics and Astronautics, 29 General Road, Jiangning District, Nanjing 211106, China
[b] Jiangsu Key Laboratory of Material and Technology for Energy Conversion, Nanjing 211106, China

ARTICLE INFO

Keywords:
X-ray radioluminescence nuclear battery
Radioluminescence spectra
GaAs device
Phosphor layers
Aluminum film

ABSTRACT

The output properties of X-ray radioluminescence (RL) nuclear batteries with different phosphor layers were investigated by using low-energy X-ray. Results indicated that the values of electrical parameters increased as the X-ray energy increased, and the output power of nuclear battery with ZnS:Cu phosphor layer was greater than those of batteries with ZnS:Ag, (Zn,Cd)S:Cu or Y_2O_3:Eu phosphor layers under the same excitation conditions. To analyze the RL effects of the phosphor layers under X-ray excitation, we measured the RL spectra of the different phosphor layers. Their fluorescence emissions were absorbed by the GaAs device. In addition, considering luminescence utilization in batteries, we introduced an aluminum (Al) film between the X-ray emitter and phosphor layer. Al film is a high performance reflective material and can increase the fluorescence reaching the GaAs photovoltaic device. This approach significantly improved the output power of the battery.

1. Introduction

Nuclear batteries have potential uses as power supplies in micro-electromechanical systems (MEMS) because they exhibit high energy density, stability, and long life [1–5]. Several investigations on nuclear batteries were conducted. Low-energy X-ray nuclear batteries are attracting widespread interest because of their excellent properties [6–8]. They can be easily shielded in contrast to γ-ray batteries and are safe because they only emit low-energy X-ray photons [9–11]. However, the semiconductor material will suffer radiation damage when exposed to intense fluxes of low-energy X-ray for a long time [12–15].

An alternative method to direct conversion of X-ray batteries is the addition of a phosphor layer and substrate, which directly absorb low-energy X-rays. Radiation energy is converted into luminescence energy, which is then converted into electricity [16–18]. Thus, the semiconductor is shielded from X-ray radiation damage. In such nuclear batteries, the phosphor layer and substrate material are exposed to X-ray irradiation, but radiation damage is slowed down because of these components [19]. Thus, low-energy X-ray radioluminescence (RL) nuclear battery can reduce radiation damage effectively. However, studies on low-energy X-ray RL nuclear batteries are rare.

The objective of this study is to investigate the characteristics of low energy X-ray RL nuclear batteries with different phosphor layers by using different low-energy X-rays. The optical properties of luminescent materials and spectral responsitivity of a GaAs device were analysed. In batteries, output power can be enhanced by increasing luminescence intensity and improving the degree of response between an RL and photovoltaic material. Moreover, output performance can be improved after loading an aluminum (Al) film on the surface of the phosphor layer. Our findings indicated that Al films can improve luminescence utilization rate.

A low-energy X-ray RL nuclear battery is composed of an X-ray source, phosphor layer, and photovoltaic material. A schematic presentation of the operating principles of the battery is shown in Fig. 1. Low-energy X-ray RL nuclear batteries utilize X-ray to produce visible luminescence in phosphor materials. The photovoltaic material receives visible luminescence from the phosphor layer and creates electron–hole pairs. These electron–hole pairs are then separated by a built-in electrical field, and the battery delivers an output current after being connected to an external circuit.

2. Materials and methods

2.1. Experimental materials

An X-ray tube (Shanghai KeyWay Electron Company Ltd., KYW900A, China) was used to simulate the low-energy X-ray source for convenience and easy adjustment of the intensity of the emitted X-rays. The basic specifications of the X-ray tube are listed in Table 1.

Under excitation condition of 10 kV tube voltage, the X-ray energy

* Corresponding author at: Department of Nuclear Science and Engineering, Nanjing University of Aeronautics and Astronautics, Nanjing, China.
E-mail address: tangxiaobin@nuaa.edu.cn (X.-B. Tang).
[1] These authors contributed to the work equally and should be regarded as co-first authors.

https://doi.org/10.1016/j.nimb.2017.10.033
Received 5 September 2017; Received in revised form 27 October 2017; Accepted 30 October 2017
0168-583X/

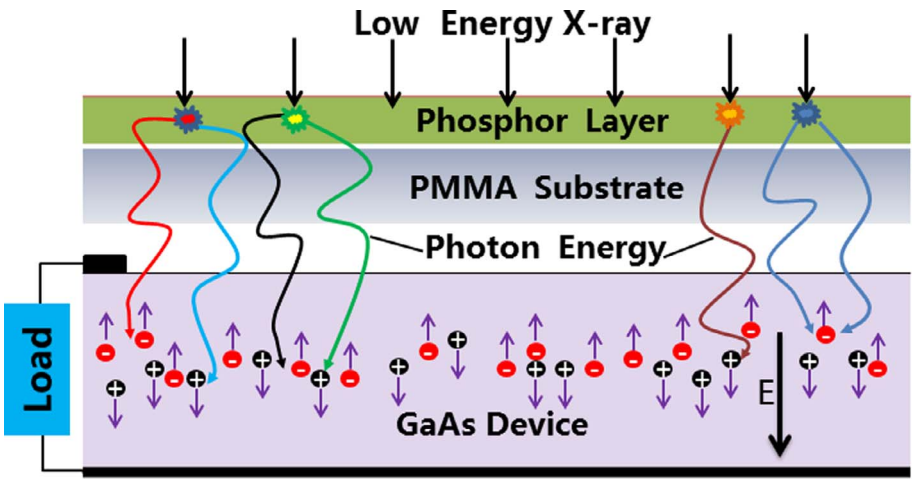

Fig. 1. Schematic of a low-energy X-ray RL nuclear battery.

Table 1
Specification of the X-ray tube.

Anode voltage	Anode current	Maximum power	Filament voltage	Filament current
50 kV	0–1 mA	50 W	2.0 V	60 kV/1 mA, I_f = 1.7 A
Thickness of the beryllium window	Target angle	Focus spot size	Grounded mode	Target
200 μm	10°	0.1 mm × 0.1 mm	Grounded-cathode	Molybdenum

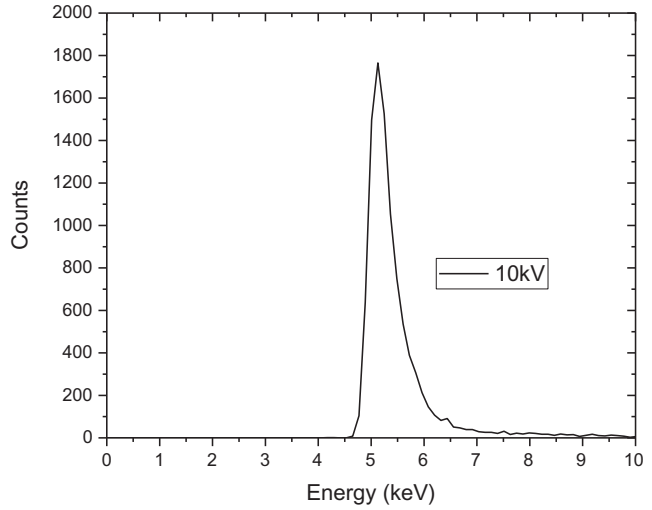

Fig. 2. X-ray energy spectrum for a tube voltage of 10 kV.

Fig. 3. Four different phosphor layers under 365 nm UV lamps (from left to right: ZnS:Ag, ZnS:Cu, (Zn,Cd)S:Cu, and Y_2O_3:Eu phosphor layers).

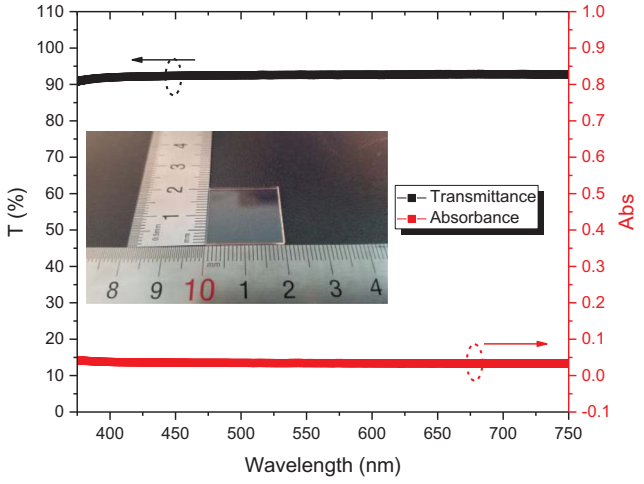

Fig. 4. Transmission and absorption spectra of the PMMA substrate.

spectrum was obtained by CdZnTe detector as shown in Fig. 2. It can be observed that the energy thereof is mainly concentrated in the middle section. The horizontal and vertical coordinates represent the photon energy and the photon numbers, respectively.

Four different phosphor layers were fabricated with ZnS:Ag, ZnS:Cu, (Zn,Cd)S:Cu, and Y_2O_3:Eu phosphor powder, and the size of each phosphor layer was 2 cm × 2 cm. The grain diameters of corresponding phosphor powders were 6.2, 38.0, 6.0, and 5.8 μm. Four different phosphor layers under 365 nm UV lamps are illustrated in Fig. 3. The colors of the phosphor layers were blue, green, yellow, and red. The ZnS:Ag, ZnS:Cu, and (Zn,Cd)S:Cu phosphor layers were more brightly colored than Y_2O_3:Eu phosphor layer as illustrated in Fig. 3.

Polymethylmethacrylate (PMMA) substrates were used as substrate materials for the phosphor layers because they have ultralight mass and exhibit good light transmittance [20,21]. The transmission and absorption spectra (Fig. 4) of the PMMA substrate were measured with an ultraviolet–visible spectrophotometer (Shimadzu UV-2550, Japan) at 375–750 nm scanning range. The values of various parameters of the PMMA substrate are listed in Table 2.

The GaAs device with compact structure [22], direct band gap structure, large light absorption coefficient, wide band gap [23,24], and high crystal quality [25] was employed in the RL nuclear battery. The active area of the GaAs device was 10 mm × 10 mm. The prototype and structure schematic of the GaAs device are illustrated in Fig. 5.

Table 2
Parameters of the PMMA substrate.

Dimensions (mm)	Mass (g)	Transmittance (%)	Absorbance
20 × 20 × 2	0.835	> 91	< 0.035

2.2. Experimental measurements

2.2.1. Electrical test

An X-ray tube was placed 2 cm above the phosphor layer, and the electrical properties of RL nuclear batteries with different phosphor layers, such as short circuit current (I_{sc}) and open circuit voltage (V_{oc}), were obtained with a dual-channel system source-meter instrument (Model 2636A, Keithley, USA) at room temperature. The maximum output power (P_{max}) and fill factor (*FF*) can be calculated by Eqs. (1) and (2) as follows:

$$P_{max} = V_{max} \times I_{max} \quad (1)$$

$$FF = \frac{V_{max} \times I_{max}}{V_{oc} \times I_{sc}} \quad (2)$$

where V_{max} and I_{max} are the voltage and current, respectively, at the maximum power point.

2.2.2. Optical test

The RL spectra of different phosphor layers under different tube voltages (10, 15, 20, 25, 30 kV) were tested with a Cary Eclipse fluorescence spectrophotometer (Agilent Technologies G9800a, Malaysia) when the tube current was 800 μA. The data mode of Cary Eclipse luminescence spectrophotometer was set as bio/chemiluminescence, and the emission slit and photomultiplier detector voltage were 20 nm and 800 V, respectively. The spectral response curve of the GaAs device was measured at room temperature by quantum efficiency spectrometer (Bentham PVE300, Britain). The electrical and optical measurement systems are shown in Fig. 6.

3. Results and discussion

3.1. Electrical characterization of nuclear battery

The tube current was set to 800 μA, and the tube voltages were set to 10, 15, 20, 25, and 30 kV, respectively. The electrical performances of the X-ray RL nuclear batteries with different phosphor layers were measured during continuous and direct X-ray exposure. The corresponding *I–V* characteristics are illustrated in Fig. 7. Both I_{sc} and V_{oc} increased significantly at increased tube voltage for four different phosphor layers.

Fig. 8 shows the changes in I_{sc}, V_{oc}, P_{max}, and *FF* for the RL nuclear batteries with different phosphor layers as a function of tube voltage (10–30 kV). Remarkable changes in the electrical performances were observed after the tube voltage was increased (Fig. 8). Obvious increases in the I_{sc}, V_{oc}, P_{max}, and *FF* values were also observed. The rate of I_{sc} and P_{max} sped up and became faster than those of V_{oc} and *FF*. The *FF* value stabilized at 25–30 kV. In Fig. 8a and c, the I_{sc} and P_{max} values of the battery with ZnS:Cu phosphor layer were greater than those of the batteries with ZnS:Ag, (Zn, Cd)S:Cu, and Y_2O_3:Eu phosphor layers at the same tube voltage. In Fig. 8b, the V_{oc} value of the battery with ZnS:Cu phosphor layer was extremely close to that of the battery with (Zn, Cd)S:Cu phosphor layer and was greater than those of batteries with ZnS:Ag and Y_2O_3:Eu phosphor layers.

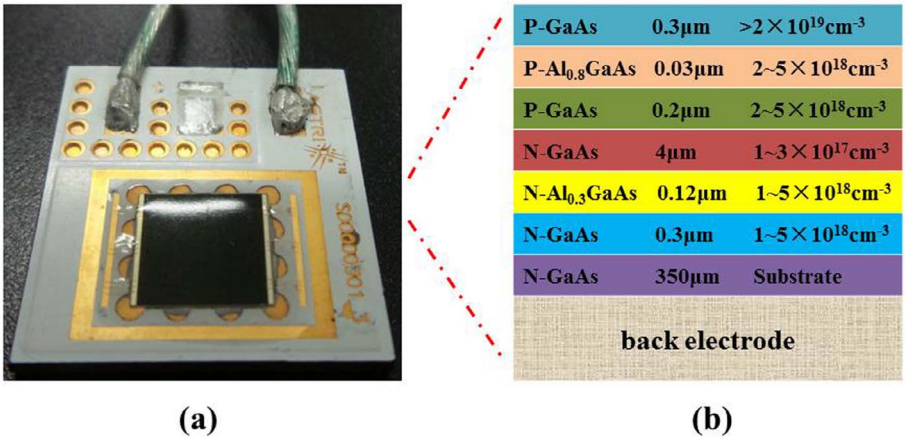

Fig. 5. (a) Prototype and (b) structure schematic of GaAs device.

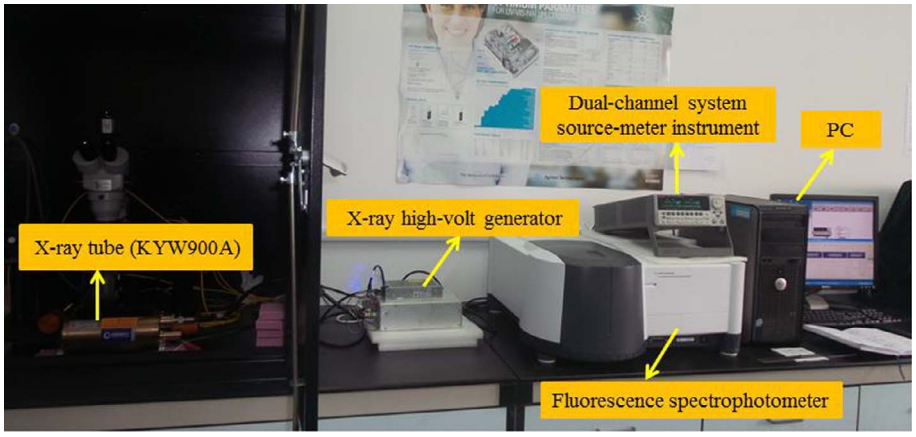

Fig. 6. Testing system for electrical performance and optical performance.

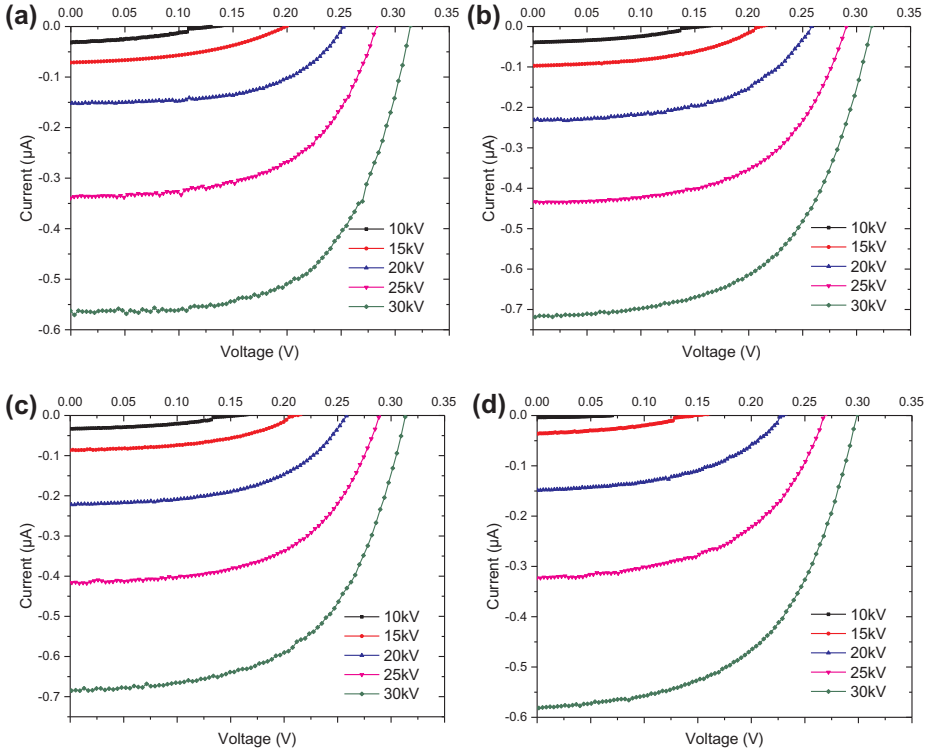

Fig. 7. *I–V* curves of the batteries with different phosphor layers under different tube voltages: (a) ZnS: Ag, (b) ZnS: Cu, (c) (Zn,Cd)S:Cu, and (d) Y_2O_3:Eu.

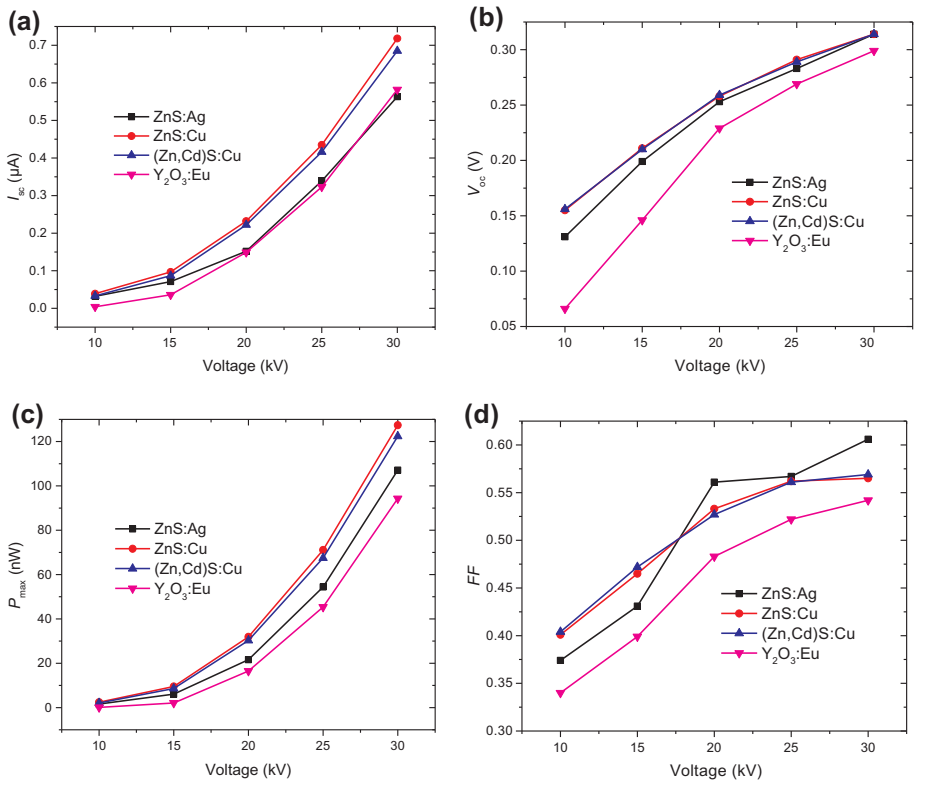

Fig. 8. Electrical properties of the RL nuclear batteries with different phosphor layers as a function of X-ray tube voltage: (a) short circuit current I_{sc}, (b) open circuit voltage V_{oc}, (c) maximum power P_{max}, and (d) fill factor *FF*.

3.2. Optical characterization of the phosphor layers

The RL spectra of the ZnS:Ag, ZnS:Cu, (Zn,Cd)S:Cu, and Y_2O_3:Eu phosphor layers under different tube voltages are provided in Fig. 9. The RL relative intensities of the phosphor layers were enhanced at increased tube voltage. However, the emission peak wavelengths of the phosphor layers remained steady and unchanged at different tube voltages. The emission peak wavelengths of ZnS:Ag, ZnS:Cu, (Zn,Cd) S:Cu, and Y_2O_3:Eu phosphor layers were approximately 450, 530, 560, and 613 nm, respectively. Besides, another emission peak wavelength

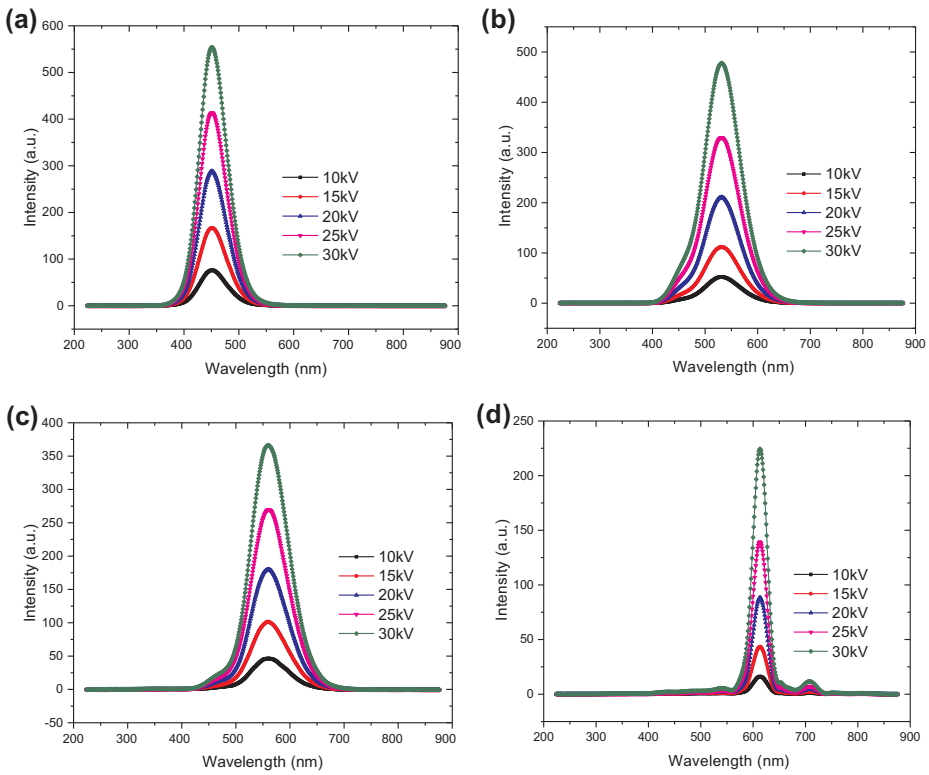

Fig. 9. RL spectra of phosphor layers under different tube voltages: (a) ZnS:Ag, (b) ZnS:Cu, (c) (Zn,Cd)S:Cu, and (d) Y_2O_3:Eu.

of the Y_2O_3:Eu phosphor layer was approximately 708 nm.

The RL spectra of ZnS:Ag, ZnS:Cu, (Zn,Cd)S:Cu, and Y_2O_3:Eu phosphor layers at the same tube voltage are all shown in Fig. 10 to facilitate comparison and analysis. The phosphor layers exhibited different emission spectra because of the presence of different luminescent materials. The RL spectra of the phosphor layers the fluorescence emissions at 375–750 nm wavelength range. The RL intensities of the ZnS:Ag, ZnS:Cu, (Zn,Cd)S:Cu, and Y_2O_3:Eu phosphor layers were weakened when the phosphor layers were subjected to the same excitation conditions. This phenomenon indicated that the ZnS:Ag and ZnS:Cu exhibit higher RL efficiencies than (Zn,Cd)S:Cu and Y_2O_3:Eu under excitation by X-rays. Furthermore, the luminescence transmissions of the phosphors with large particle sizes were significant and effective. This finding was mentioned in Ref. [26], and the scattering coefficient (s) can be calculated as follows:

$$\ln s = \ln k - \ln g + 0.5 \ln^2 J, \tag{3}$$

where k is a constant, g is the average particle size of the phosphors, and J is the standard deviation of g. According to the formula, as the average particle size g increases, and the scattering coefficient s decreases, which eventually leads to an increased luminescence transmission efficiency.

3.3. Degree of spectral matching between the phosphor layers and GaAs device

The spectral response curves of the GaAs device and the RL spectra of different phosphor layers are shown in Fig. 11. The GaAs device can offer high responsibility and wide spectrum. The external quantum efficiency of the GaAs device was 80%–94% at a wavelength range of 500–750 nm, where light was absorbed efficiently by the GaAs device. However, when the phosphor layer emitted RL with a range of 375–450 nm, the external quantum efficiency of the GaAs device was only 19%–74%. Therefore, a good match between the RL spectra of ZnS:Cu, (Zn,Cd)S:Cu, and Y_2O_3:Eu phosphor layers and the spectral response of the GaAs device were observed. This finding indicated that the ZnS:Cu, (Zn,Cd)S:Cu, and Y_2O_3:Eu phosphor layers are more suitable than ZnS:Ag to couple with the GaAs device.

3.4. Battery enhanced by introducing the Al film

Considering the RL utilization and the performance output of battery, one possible method is to introduce a thin Al film between the X-ray emitter and phosphor layer. Al film is a reflector which is thin enough so that it does not stop the low energy x-rays but thick enough so that it can reflect the light from the phosphors. The aim of this method is to reduce luminescent loss and increase luminescence availability. The structure schematic and prototype of the battery are shown in Figs. 12 and 13. An Al film of 10 μm thickness was loaded on a phosphor layer, and the batteries were excited by an X-ray tube. The tube voltage was set to 30 kV, and the tube current was set to 800 μA. Fig. 14 shows the I–V and P–V characteristic curves of the GaAs low-energy X-ray RL nuclear batteries before and after loading the Al film, and the corresponding electrical parameters are illustrated in Table 3.

As shown in Fig. 14, the I_{sc} and P_{max} values of batteries with ZnS:Ag, ZnS:Cu, and (Zn,Cd)S:Cu increased obviously after loading the Al film. However, in the batteries with Y_2O_3:Eu, the I_{sc} and P_{max} values decreased slightly after loading the Al film. The amount of luminescence that entered PV material was affected by X-ray energy and luminescent utilization. Excited by X-rays, the phosphor layer

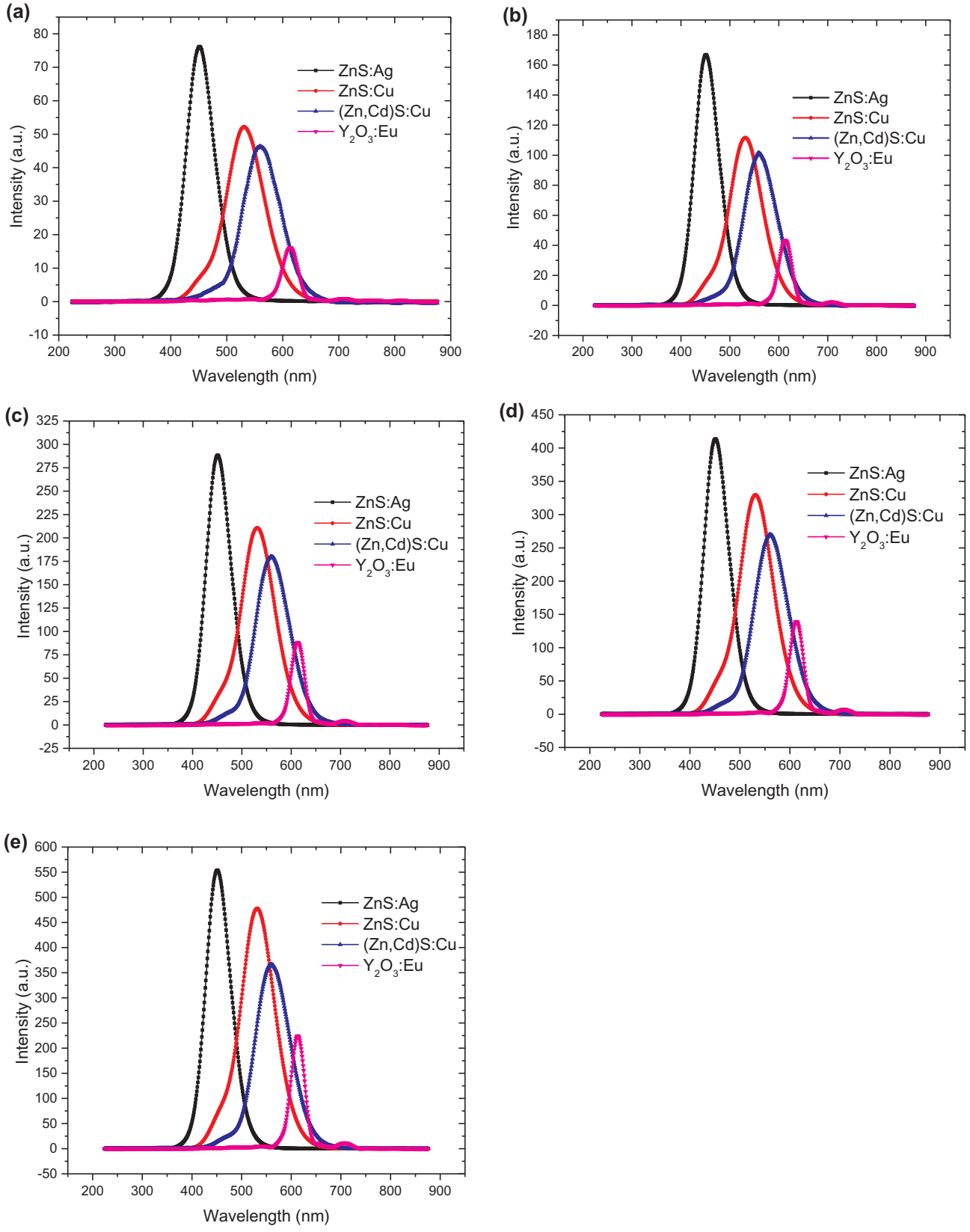

Fig. 10. RL spectra of different phosphor layers under excitation by (a) 10, (b) 15 kV, (c) 20, (d) 25, and (e) 30 kV tube voltages.

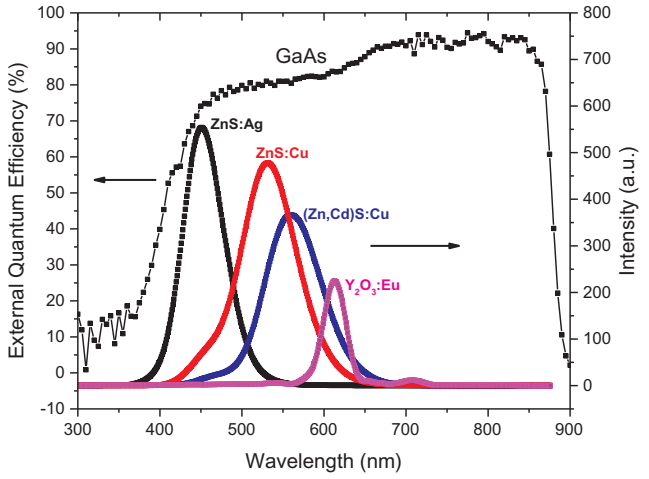

Fig. 11. Spectral response curves of the GaAs device and RL spectra of different phosphor layers under excitation by 30 keV.

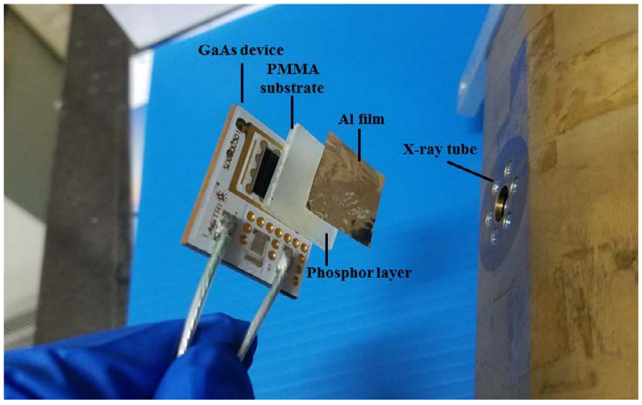

Fig. 13. Prototype of the GaAs X-ray RL nuclear battery enhanced by the Al film.

generated visible luminescence. The light emission of the phosphor layer was isotropic, and the intensity of the light emitted toward the X-ray emitter was equal to that emitted toward the GaAs device. The Al film is an excellent reflective material and can increase luminescent flux on the GaAs device by reflecting the luminescence emitted toward an X-ray emitter. In the phosphor layers, the Al film blocked the X-rays and reduced their energies. In other words, the RL intensity from the phosphor layer was reduced to some extent. In the batteries with ZnS:Ag, ZnS:Cu, and (Zn,Cd)S:Cu phosphor layers, the photon reflection-increase effect of the Al film was stronger than it's X-ray-blocking capability. However, the photon reflection-increase effect was weaker than X-ray-blocking capability for battery with Y_2O_3:Eu phosphor layer.

In Table 3, P_{max} values of the batteries with ZnS:Ag and (Zn,Cd)S:Cu increased by 5.23% and 15.77%, respectively, after the Al film was loaded. Especially for the battery with ZnS:Cu, P_{max} increased by 34.22% after loading the Al film. However, P_{max} of the battery with Y_2O_3:Eu decreased by 6.79% after loading the Al film.

4. Conclusions

The GaAs low energy X-ray RL nuclear battery was investigated under different low energy X-rays. In this proof of concept experiment, the output performance of the battery was largely determined by RL wavelength and RL intensity. The results showed that the RL relative intensity increased as the tube voltage increased for the phosphor layers. The ZnS:Cu is more suitable than ZnS:Ag for coupling with the GaAs device, and a good match between the RL spectra of ZnS:Cu phosphor layers and the spectral response of the GaAs device was observed. In addition, ZnS:Cu exhibited higher RL efficiency than (Zn,Cd)S:Cu and Y_2O_3:Eu under X-ray excitation. The I_{sc} and P_{max} values of the battery with ZnS:Cu phosphor layer were greater than those with ZnS:Ag, (Zn, Cd)S:Cu, and Y_2O_3:Eu phosphor layers under the same excitation conditions. The Al film was loaded into the surface of the phosphor layers to increase the availability of luminescence. After loading, the output power of the batteries significantly improved, except that of the battery with Y_2O_3:Eu phosphor layer. Therefore, Al film can be used in X-ray RL nuclear batteries, and it can improve output performance.

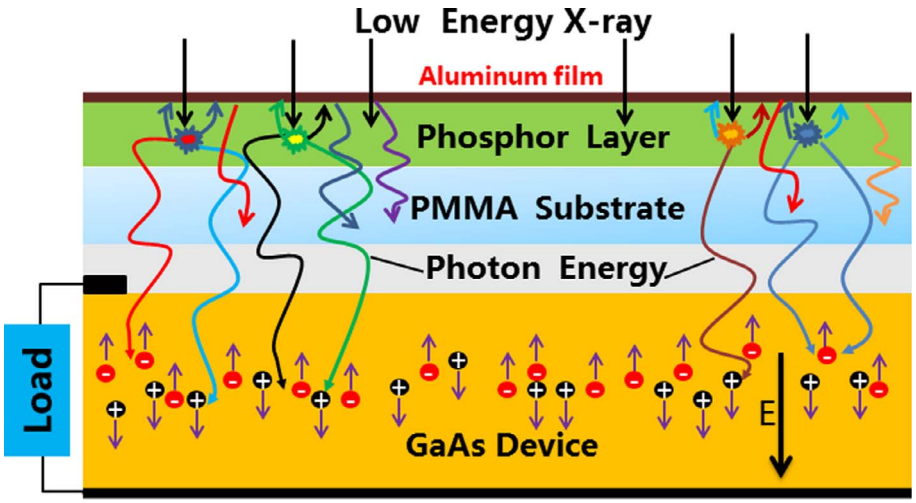

Fig. 12. Schematic of the GaAs X-ray RL nuclear battery enhanced by the Al film.

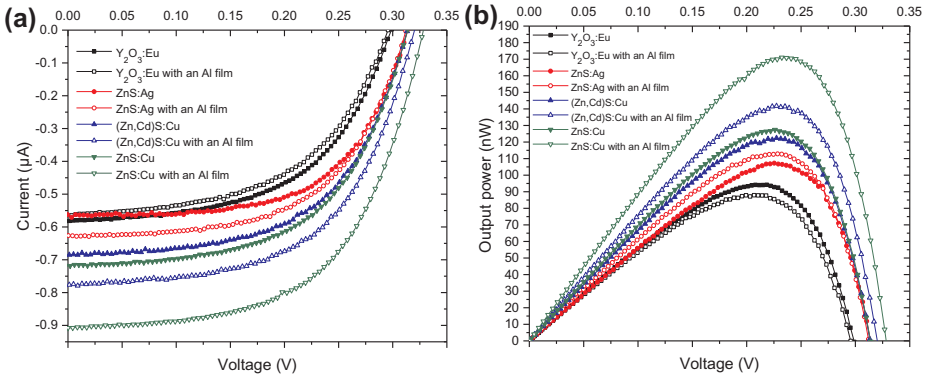

Fig. 14. *I–V* (a) and *P–V* (b) curves of the batteries of the GaAs X-ray RL nuclear batteries before and after loading Al film.

Table 3
Electrical parameters of the GaAs X-ray RL nuclear batteries before and after loading Al film.

Phosphor layers	ZnS:Ag	ZnS:Ag + Al film	ZnS:Cu	ZnS:Cu + Al film	(Zn,Cd)S:Cu	(Zn,Cd)S:Cu + Al film	Y_2O_3:Eu	Y_2O_3:Eu + Al film
I_{sc} (μA)	0.563	0.626	0.718	0.908	0.685	0.777	0.582	0.564
V_{oc} (V)	0.314	0.312	0.314	0.328	0.314	0.320	0.299	0.296
P_{max} (nW)	107.1	112.7	127.4	171	122.4	141.7	94.3	87.9
FF	0.606	0.577	0.565	0.574	0.569	0.570	0.542	0.527

Acknowledgements

This work was supported by the National Natural Science Foundation of China (Grant Nos. 11675076 and 11505096), the Natural Science Foundation of Jiangsu Province (Grant No. BK20150735), the Shanghai Aerospace Science and Technology Innovation Project (Grant No. SAST2016112), the National Defense Basic Scientific Research Project (Grant No. JCKY2016605C006) and the Priority Academic Program Development of Jiangsu Higher Education Institutions.

References

[1] M.A. Prelas, C.L. Weaver, M.L. Watermann, E.D. Lukosi, R.J. Schott, D.A. Wisniewski, A review of nuclear batteries, Prog. Nucl. Energy 75 (2014) 117–148.
[2] Y. Liu, X. Tang, Z. Xu, L. Hong, D. Chen, Experimental and theoretical investigation of temperature effects on an interbedded betavoltaic employing epitaxial Si and bidirectional ^{63}Ni, Appl. Radiat. Isot. 94 (2014) 152–157.
[3] D.Y. Qiao, X.J. Chen, Y. Ren, W.Z. Yuan, A micro nuclear battery based on SiC schottky barrier diode, J. Microelectromech. Syst. 20 (2011) 685–690.
[4] J. Russo, M. Litz, W. Ray, G.M. Rosen, D.I. Bigio, R. Fazio, Development of tritiated nitroxide for nuclear battery, Appl. Radiat. Isot. 125 (2017) 66–73.
[5] A. Sharma, J. Melancon, S.G. Bailey, S. Zivanovic, Novel use of semiconductive conjugated polymer with optimized scintillator for betavoltaic applications, ASME 2015 IMECE Vol. 6B Energy. (2015) V06BT07A041.
[6] S. Butera, G. Lioliou, A.M. Barnett, Gallium arsenide ^{55}Fe X-ray-photovoltaic battery, J. Appl. Phys. 119 (2016) 064504.
[7] S. Butera, G. Lioliou, A.B. Krysa, A.M. Barnett, $Al_{0.52}In_{0.48}P$ ^{5}5Fe x-ray-photovoltaic battery, J. Phys. D, Appl. Phys. 49 (2016) 355601.
[8] G. Lioliou, M.C. Mazzillo, A. Sciuto, A.M. Barnett, Electrical and ultraviolet characterization of 4H-SiC Schottky photodiodes, Opt. Express 23 (2015) 21657–21670.
[9] G. Lioliou, X. Meng, J.S. Ng, A.M. Barnett, Article : Temperature dependent characterization of Gallium Arsenide X-ray mesa p-i-n photodiodes, 119 (2016) 124507.
[10] S. Butera, M.D.C. Whitaker, G. Lioliou, A.M. Barnett, AlGaAs ^{55}Fe X-ray radioisotope microbattery, Sci. Rep. 6 (2016) 38409.
[11] Z.R. Zhang, X. Bin Tang, Y.P. Liu, Z.H. Xu, Z.C. Yuan, K. Liu, W. Chen, GaAs radiovoltaic cell enhanced by Y_2SiO_5 crystal for the development of new gamma microbatteries, Nucl. Instrum. Methods Phys. Res. B 398 (2017) 35–41.
[12] G. Li, Y. Yang, R.aB. Devine, C. Mayberry, Radiation induced damage and recovery in poly(3-hexyl thiophene) based polymer solar cells, Nanotechnology 19 (2008) 424014.
[13] Y. Lei, Y. Yang, Y. Liu, H. Li, G. Wang, R. Hu, X. Xiong, S. Luo, The radiation damage of crystalline silicon PN diode in tritium beta-voltaic battery, Appl. Radiat. Isot. 90 (2014) 165–169.
[14] J.M. Benedetto, H.E. Boesch, The relationship between ^{60}Co and 10-keV X-ray damage in MOS devices, IEEE Trans. Nucl. Sci. 33 (1986) 1317–1323.
[15] D.M. Fleetwood, P.S. Winokur, C.M. Dozier, D.B. Brown, Effect of bias on the response of metal-oxide-semiconductor devices to low-energy x-ray and cobalt-60 irradiation, Appl. Phys. Lett. 52 (1988) 1514–1516.
[16] Z.H. Xu, X.B. Tang, L. Hong, et al., Development of a beta radioluminescence nuclear battery, Nucl. Sci. Tech. 25 (4) (2014) 79–84.
[17] L. Hong, X. Bin Tang, Z.H. Xu, Y.P. Liu, D. Chen, Radioluminescent nuclear batteries with different phosphor layers, Nucl. Instrum. Methods Phys. Res. B 338 (2014) 112–118.
[18] X. Bin Tang, L. Hong, Z.H. Xu, Y.P. Liu, D. Chen, Temperature effect of a radioluminescent nuclear battery based on ^{147}Pm/ZnS: Cu/GaAs, Appl. Radiat. Isot. 97 (2015) 118–124.
[19] R. Walton, C. Anthony, M. Ward, N. Metje, D.N. Chapman, Radioisotopic battery and capacitor system for powering Wireless Sensor Networks, Sensors Actuators A Phys. 203 (2013) 405–412.
[20] F. Therriault-Proulx, L. Beaulieu, L. Archambault, S. Beddar, On the nature of the light produced within PMMA optical light guides in scintillation fiber-optic dosimetry, Phys. Med. Biol. 58 (2013) 2073.
[21] J. Hu, Y. Zhou, M. He, X. Yang, Novel multifunctional microspheres of polysiloxane@CeO_2-PMMA: optical properties and their application in optical diffusers, Opt. Mater. (Amst) 36 (2013) 271–277.
[22] H. Wang, X. Tang, Y. Liu, Z. Xu, M. Liu, D. Chen, Temperature effect on betavoltaic microbatteries based on Si and GaAs under ^{63}Ni and ^{147}Pm irradiation, Nucl. Inst. Methods Phys. Res. B 359 (2015) 36–43.
[23] S.M. Sze, K.K. Ng, Physics of Semiconductor Devices, John Wiley & Sons, 2006.
[24] W.J. Choyke, G. Pensl, Physical properties of SiC, MRS Bull. 22 (03) (1997) 25–29.
[25] S. Butera, G. Lioliou, A.M. Barnett, Temperature effects on gallium arsenide ^{63}Ni betavoltaic cell, Appl. Radiat. Isot. 125 (2017) 42–47.
[26] K.H. Butler, Fluorescent Lamp Phosphors: Theory and Technology, Pennsylvania State, Pennsylvania State University Press, USA, 1980, pp. 132–168.